Regulation of rheumatoid arthritis microenvironment *via* a self-healing injectable hydrogel for improved inflammation elimination and bone repair

Wenbo Geng [a,1], Jie Zhao [b,1], Bailong Tao [c], Yulu Yang [a], Qiaojian Duan [a], Pengfei Gao [a], Tingting He [a], Shaopeng Liu [a], Qian Feng [a], Peng Zhao [a,**], Kaiyong Cai [a,*]

[a] *Key Laboratory of Biorheological Science and Technology, Ministry of Education College of Bioengineering, Chongqing University, Chongqing, 400044, PR China*
[b] *College of Medicine and Life Sciences, Chengdu University of Traditional Chinese Medicine, Chengdu, 611137, Sichuan, PR China*
[c] *Laboratory Research Center, The First Affiliated Hospital of Chongqing Medical University, Chongqing, 400016, PR China*

ARTICLE INFO

ABSTRACT

The rheumatoid arthritis (RA) microenvironment is often followed by a vicious circle of high inflammation, endogenous gas levels imbalance, and poor treatment. To break the circle, we develop a dual-gas-mediated injectable hydrogel for modulating the immune microenvironment of RA and simultaneously releasing therapeutic drugs. The hydrogel (DNRS gel) could be broken down on-demand by consuming excessive nitric oxide (NO) and releasing therapeutic hydrogen sulfide (H_2S), resulting in endogenous gas restoration, inflammation alleviation, and macrophage polarization to M2 type. Additionally, the hydrogel could suppress osteoclastogenesis and enhance osteogenesis. Furthermore, the intra-articularly injected hydrogel with methotrexate (MTX/DNRS gel) significantly alleviated inflammation and clinical symptoms and promoted the repair of bone erosion in the collagen-induced arthritis rat model. As a result, *in vivo* results demonstrated that MTX/DNRS gel restored the microenvironment and improved the therapeutic effect of MTX. This study provides a novel understanding of developing versatile smart delivery platforms for RA treatment.

1. Introduction

Rheumatoid arthritis is one of the most autoimmune diseases affecting ~1% population worldwide characterized by erosion of periarticular bone, synovitis, and osteoporosis [1–5]. Patients with advanced RA severely affect their quality of life and physical function [6]. In the past years, the current clinical treatments of RA drugs have been focused on reducing inflammation [7,8]. However, these drugs often cause drug resistance, undesired long-term side effects, and recurrence of RA [3,9–11]. Thus, it is important to search for safe and effective approaches to inhibit acute inflammation and bone erosion for RA treatment.

Endogenous gases (such as NO and H_2S) play a critical in the regulation of RA microenvironment, but these gases are highly concentration-dependent [12–15]. Excessive NO and insufficient H_2S could cause inflammation and activate osteoclasts to dissolve the bone tissue, which delays bone healing and exacerbates RA [13,16–18].

Therefore, gas-mediated therapy has been employed to manage the RA microenvironment [19]. However, most gas-mediated therapeutic materials are in the nanoscale range, which makes them prone to diffuse to other tissues from the injection sites, leading to unnecessary changes of endogenous gas levels in non-inflammatory tissues. Additionally, nanomaterials are often easily cleared and require high doses of repetitive conduct, which may cause systemic toxicity, aggravate patient pain, and increase infection risk.

Injectable hydrogels that can form gels in situ have been widely used in biomedical applications, such as cell/drug delivery and tissue engineering [20,21]. These hydrogels can be designed to respond to physiological conditions., and thereby control drug release therefore increasing the therapeutic effect [12,22,23]. Moreover, Hydrogels also adapted to the local characteristics of bone defects and withstand shear and tension forces, and can also act as lubrication [24]. However, chemically cross-linked hydrogels often require the introduction of highly toxic catalysts or initiators, which limits their application [25].

Hence, a low-toxicity hydrogel with gas-mediated function in the RA microenvironment can potentially enhance the treatment of bone erosion in RA.

Herein, we devised a self-healing injectable hydrogel (which could deplete NO and release H_2S, and is named DNRS gel) for RA treatment through combining a thiol-modified hyaluronic acid (HA-SH) with dual-gas-mediated crosslinker by metal-free biorthogonal click reaction (Scheme 1). DNRS hydrogels possess the following advantages: 1) The HA component of DNRS hydrogels provides self-healing lubricating effect and can reduce the number of injections; 2) DNRS hydrogels can scavenge excess NO and release anti-inflammatory gas H_2S, improving the RA microenvironment and further regulating bone metabolism to promote bone regeneration; 3) The hydrogel can effectively load hydrophobic drugs and release them in response, ultimately enhancing the treatment of RA through a synergistic effect. Therefore, our strategy

provides a promising, essential insight into the design and biological mechanisms of hydrogel for treating inflammatory bone erosion.

2. Materials and methods

2.1. Materials

Carbon disulfide, chloroform, dimethyl sulphoxide (DMSO), acetonitrile, acetone, $SOCl_2$, dichloromethane, tetrahydrofuran, ethyl acetate. tetrabutylammonium hydrogen sulfate, o-phenylenediamine, 2,2′-Azobis(2-methylpropionitrile) (AIBN), propynol ethoxylate, N,N-dimethyl-p-phenylene diamine 1-ethyl-3-(3-(dimethylamino)propyl) carbodiimide (EDC·HCl), Tris(2-carboxyethyl) phosphine hydrochloride (TCEP-HCl), 3,3′-dithiobis(propanoic dihydrazide) (DTPHY) were purchased from Sinopharm Chemical Reagent Co., Ltd (Shanghai, China). Poly
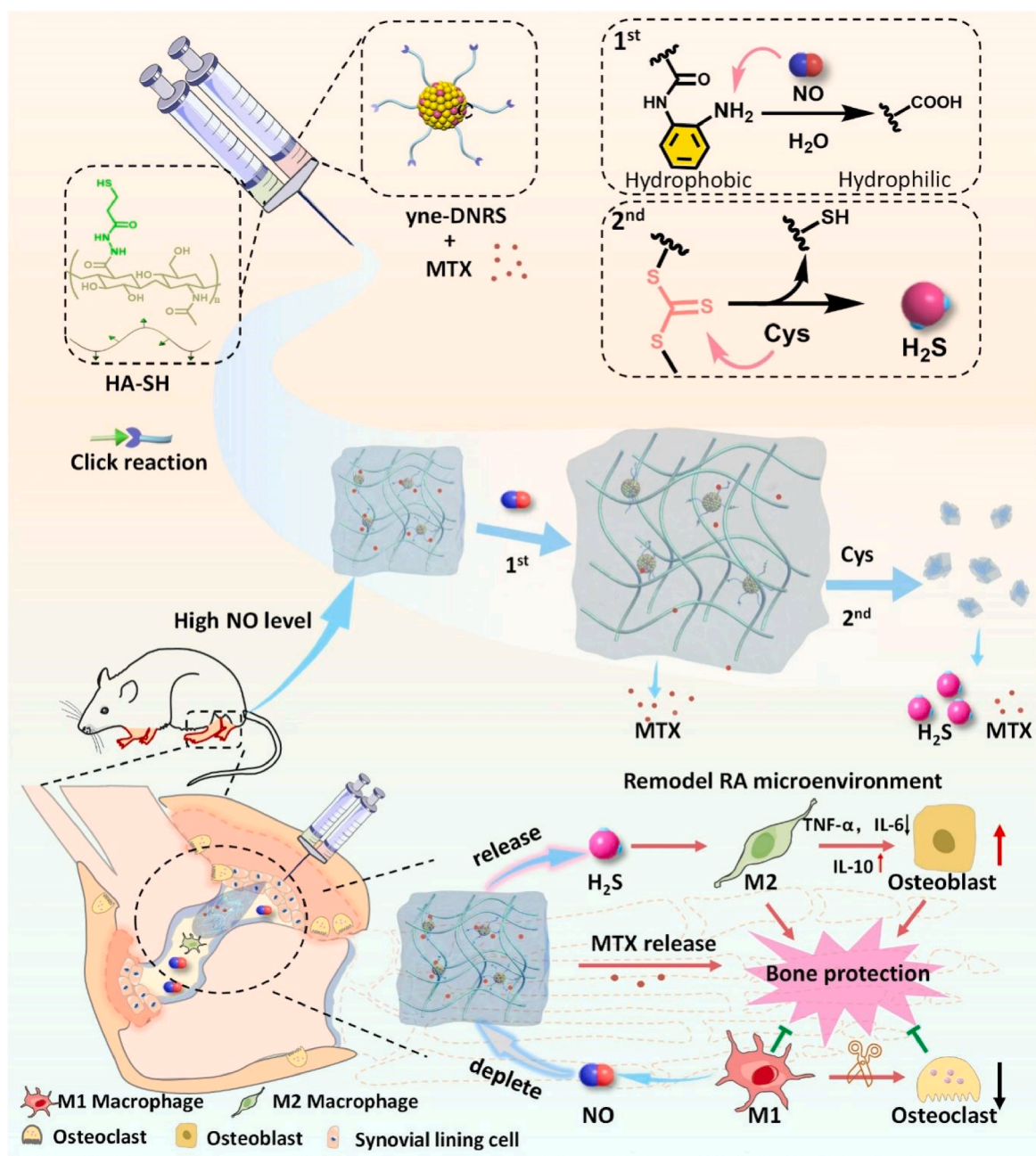
Scheme 1. Schematic illustration of the fabrication of self-healing injectable hydrogel and the mechanism of bone protection by regulating the microenvironment of RA. DNRS gel depletes excessive NO and releases H_2S in the presence of cysteine, and sustained release MTX.

(ethylene glycol) methyl ether acrylate(pegma, Mn = 480), HA sodium salt, lipopolysaccharide (LPS) and griess reagent were purchased from Sigma-Aldrich (St. Louis, MO, USA), WSP-5 and DAF-2 were obtained from APExBIO Technology LLC (Houston, USA). RANKL and m-CSF were purchased from Peprotech Inc.

2.2. Characterization

^{1}H NMR spectra were recorded on a Bruker nuclear magnetic resonance spectrometer (400 MHz, Switzerland). TEM was conducted on a JEOL 2010 electron microscope (120 kV). The molecular weight of the polymers was measured by gel permeation chromatography (GPC) using a Waters 1515 GPC. Nanoparticle size distribution was assessed by a Malvern Zetasizer Nano ZS90. The micro-CT images were scanned by CT-35 scanner (SCANCO Medical, Switzerland). CLSM images were acquired by a Leica TCS SP5 microscope.

2.3. Synthesis of yne-BDATC (H$_2$S donor and RAFT agent)

S,S′-Bis(α,α′-dimethyl-α′′-acetic acid) trithiocarbonate (BDATC) was synthesized according to the reported literature [26]. Yne-BDATC was synthesized via the esterification of BDATC with propynol ethoxylate. Briefly, 40 mL of SOCl$_2$ containing 1.56 g of BDATC was added to the mixture. After reacting at 60 °C for 3 h, then SOCl$_2$ was removed by rotary evaporation, and adding the resultant reactant to 20 mL of dichloromethane. Then the solution was added to 30 mL of cold dichloromethane containing 2 mL pyridine and 6.2 g propargyl alcohol. After reacting at room temperature for 24 h, the solution was washed with pH = 3 HCl and water, then dried with sodium sulfate. 1.6 g of crude product was obtained after removing dichloromethane by rotary evaporation, the purified yne-BDATC was obtained as yellow oil after being purified by column chromatography (petroleum ether and ethyl acetate in a ratio of 5:1 as eluents).

2.4. The preparation of depleting NO and releasing H$_2$S (DNRS) copolymer

DNRS copolymer was synthesized according to our reported literature [27]. Step 1: Macro symmetrical trithiocarbonate chain transfer agent (CTA) agent was synthesized via RAFT polymerization with yne-BDATC as RAFT agent and AIBN as an initiator. Macro-CTA was prepared with molar ratios pegma: yne-BDATC: AIBN as 10: 0.4: 0.08. pegma (10 mmol), yne-BDATC (0.4 mmol), AIBN (0.08 mmol) were dissolved in 10 mL acetonitrile. After three freeze–pump–thaw cycles, the mixture was heated to 70 °C for 7 h. Then the mixture was quickly cooled to terminate the reaction and precipitated in cold diethyl ether. The obtained macro-CTA was used as RAFT agents. Step 2: Typically, the macro chain transfer agent (macro-CTA, 0.2 mmol), NO-responsive N-(2-aminophenyl) acrylamide hydrochloride (6 mmol), and AIBN (0.08 mmol) were dissolved in 10 mL acetonitrile. After three freeze-pump-thaw cycles, the mixture was heated to 70 °C for 7 h. Then the mixture was quickly cooled to terminate the reaction and precipitated in cold diethyl ether. DNRS copolymer was obtained as light orange solid (1.92 g). The purified product was characterized by ^{1}H NMR and GPC (Mn = 10510 Da, Mw/Mn = 1.22).

2.5. Synthesis of HA-SH

Briefly, 1.5 g of (80 kDa) and 160 mg of 3,3′-dithiobis (propanoic dihydrazide)) were dissolved in 150 mL 150 mM MES solution. Then, 270 mg of EDC·HCl was added dropwise with stirring. The reaction continues overnight. Then, 2 mL of aqueous solution containing 680 mg TCEP-HCl was added to the above solution and the reaction was allowed to continue overnight. Finally, 3.6 g of NaCl was added to the solution, dialyzed in pH 4.5 for three days, and lyophilized to obtain a white solid (~78%).

2.6. The preparation of hydrogel

DNRS hydrogel was prepared with HA-SH and DNRS copolymer in water to reach the final weight fraction of 3.0 wt% and 0.05 wt% at room temperature. Control hydrogel was prepared by replacing DNRS copolymer with alkyne-PEG-alkyne.

2.7. Mechanical properties of hydrogels

After measuring the initial weight of the hydrogel, the hydrogel was placed in different solutions and weighed to measure the weight change of the hydrogel with time. The swelling rate was calculated according to the following equation:

$$\text{Swelling ratio} = (M_f - M_i)/M_i$$

$$\text{Relative swelling ratio} = (\text{swelling ratio}) / (\text{initial swelling ratio})$$

M_f and M_i represent the weight of the hydrogel dissolved in different solutions and the weight of the dried hydrogel.

Rheology: A parallel hydrogel plate (25 mm diameter, same area as the rheometer plate probe, 1 mm thickness, consistent with the rheological test GAP setting) was placed on the carrier table of the rheometer (Anton Paar GmbH, MCR 302) and the plate probe was lowered to the set position to test the dynamic rheological properties. The stress was set to 20 Pa, angular frequency was 10 rad s^{-1}, the stress frequency was set to 1 Hz, the shear strain was 0.5%, the temperature was 25 °C or 37 °C and pH = 7.4 or 5.5.

2.8. NO-depleting and H$_2$S-releasing ability of the hydrogel

200 μL of DNRS gel was incubated in 5 mL of NO solutions (40 μM) and cysteine (100 μM), respectively. Then the NO assay kits (Griess assay) and H$_2$S probe (WSP-5) were used to test the NO-depleting and H$_2$S-releasing ability of the hydrogel according to our reported method [27].

2.9. Drug-release profile of the DNRS gel

The hydrophobic model drug MTX was encapsulated into the DNRS copolymer within the hydrogel on formation. 200 μL of DNRS gel was incubated in 5 mL of NO solutions (40 μM) or cysteine (100 μM). 500 μL of solution was removed at predetermined time intervals and replaced with the same solution. the solution was measured using a fluorescence spectrophotometer after centrifugation. The fluorescence was quantified using an excitation wavelength of 543 nm and an emission wavelength of 598 nm.

To determine MTX loading content and loading efficiency, freeze-dried MTX/DNRS gel was dissolved in water, and the absorbance at 208 nm was measured using NanoDrop 2000 spectrophotometer. The MTX concentration was calculated using a standard curve. Drug loading and encapsulation efficiency were calculated as follows:

$$\text{Loading content (\%)} = \text{weight of MTX in gels/ (weight of MTX/DNRS gel)} \times 100\%$$

$$\text{Loading efficiency (\%)} = \text{weight of MTX in gels/weight of MTX infeed} \times 100\%$$

2.10. Evaluation of cell viability

RAW 264.7 and osteoblasts were purchased from Chongqing Biospes Co., Ltd (Chongqing, China), the cell viability upon the treatment with DNRS gel and Ctrl gel were measured by CCK-8 assay and live/dead staining. Briefly, RAW 264.7 was seeded in 96-well plates in DMEM high glucose medium (10% FBS, 1% penicillin/streptomycin) with 5% CO$_2$ at

37 °C for 24 h. The gel with the same volume was added to the cells. After 24 h the cells were incubated with CCK-8 (10% volume) at 37 °C for 1 h, the absorbance of medium was detected with a microplate reader at 450 nm wavelength. The pictures of the living cells (green) and dead cells (red) were taken using fluorescence microscope.

2.11. NO-scavenging and H_2S-releasing ability in vitro

The extracellular level of NO and H_2S after treatment of DNRS gel and Ctrl gel were evaluated by DAF-2 DA and WSP-5 in RAW 264.7 macrophage cell. In brief, cells (50,000 cells/well) were seeded on 6-well plate for 24 h. After that, medium was replaced by 1 mL fresh medium, LPS (100 ng/mL), LPS (100 ng/mL)/Ctrl gel (0.5 mg/mL), and LPS (100 ng/mL)/DNRS gel (0.5 mg/mL) medium, for 24 h. The fresh medium containing DAF-2 DA (5 μM) or WSP-5 (10 μM) was added and incubated for 40 min under dark condition. Then, the culture plate was washed with PBS 3 times and fresh medium was added. The images were taken by CLSM (TCS SP5, Leica, Germany). The red channels of WSP-5 were excited at 502 nm and collected at 525 nm, the green channels of DAF-2 DA were excited at 491 nm and collected at 513 nm. For quantification of intracellular NO and H_2S concentrations of different groups was used image J.

2.12. Detection of the pro-inflammatory ability in vitro

RAW 264.7 cells were cultured were seeded on the 24-well plate for 24 h. After that, medium was replaced by 1 mL fresh medium, LPS (100 ng/mL), LPS (100 ng/mL)/Ctrl gel (0.5 mg/mL) and LPS (100 ng/mL)/DNRS gel (0.5 mg/mL) medium for 24 h. IL-6, TNF-α, and IL-10 in LPS-primed macrophage cells were detected with mouse IL-6, TNF-α, and IL-10 (MultiSciences Bio, China) mouse ELISA test kits. The absorbance was detected at 450 nm. In addition, the cells were stained with anti CD86 PE and CD206 APC for macrophage polarization experiments. The CD206 and CD86 expression were also measured by flow cytometry.

Furthermore, cells were collected after coincubation with DNRS gel and whole RNA was extracted for RNA sequencing analysis. Negative controls were LPS-treated macrophages. Sequencing work was carried out by Shanghai Majorbio Bio-pharm Technology Co., Ltd.

2.13. Osteogenic gene expression in cell culture-conditioned medium

Firstly, RAW264.7 cells were activated by LPS and treated with different samples as described above. Next, the medium was collected and centrifuged for 10 min. Afterward, the solution was mixed with DMEM medium at a volume ratio of 1:1 to form a conditioned medium. Then, the osteoblasts were inoculated with the conditioned medium. ALP expression and mineralization capacity in osteoblasts cultured with different conditioned media of culture were stained and imaged by microscopy. And the ALP expression and mineralization capacity in osteoblasts were measured according to product manuals.

2.14. Osteoclast differentiation

For osteoclast generation, RAW264.7 cells were cultured with RANKL and m-CSF for 4 days. Meanwhile, the cells were treated with different samples. Then the TRAP activity was measured by a TRAP assay kit. Meanwhile, the cells were observed with CLSM.

2.15. Animal model induction and treatment

All animal procedures were approved by Chongqing University's Laboratory Animal Welfare and Ethics Committee (CQU-IACUC-RE-202205-001). CIA model was established in six-week-old male SD rats. Briefly, 200 μL of emulsified solution (IFA and bovine type II collagen 1:1, v/v) was injected at the base of the tail. After 7 days, 100 μL of emulsified solution was given to boost the immune. 14 days after the

first immunization, five groups of CIA rats were treated with saline, MTX (0.5 mg/kg), DNRS gel (20 μL), and MTX/DNRS gel (20 μL) by intra-articular injection respectively.

2.16. Histological assay

The paw tissues were immersed in 4% paraformaldehyde for 2 days and were additionally decalcified with 15% EDTA pH 7.2 for 40 days. The decalcified tissues were embedded in wax and sectioned at 7 μm. Tissue sections were stained with hematoxylin and eosin (H&E) and Masson's trichrome. Immunohistochemical (IHC) staining of TNF-α and IL-6, and immunofluorescent of CD86 and CD206 were also performed according to the instructions. Subsequently, the histological score of synovitis and cartilage degradation were assessed according to the standard scoring method [12].

2.17. Clinical scores, swelling, temperature, and rotational cage test

The clinical score was categorized as follows (scale 0–5) according to the standard evaluation process [28]. Scores: 0, normal; 1, Minimal diffuse redness or swelling of the ankle or wrist; 2, Mild redness or swelling; 3, Moderate redness or swelling; 4, Severe redness and swelling of the entire paw; 5, Extremely inflamed limb with involvement over the entire paw.

The swelling volume of each paw was measured as our previous described [29]. Briefly, The swelling of rats' paws was measured by a devices (Fig. S1), which connecting a three-way stopcock to a 5 mL syringe, a 2 mL pipette, and a 5 mL syringe. Each rat's paw was marked, and the hindpaws were placed into the 5 mL syringe. Spilled water was collected with the 5 mL syringe, and water was slowly pumped into the 2 mL pipette. Then the swollen volume of hindpaws of rats was obtained. Thermographic images and temperature of the hindpaws were obtained by infrared thermography (FLIR e5, USA). The move ability of different groups of treated rats was placed in a rotatable cage, and recorded the number of revolutions of the rats' movement for 24 h.

2.18. Evaluation of NO, H_2S, and pro-inflammatory cytokine levels

The level of extracellular cytokines (IL-6, TNF-α, and IL-10) in the serum and tissue was evaluated by ELISA kit according to manufacturer's protocol. The foot tissue fluids were prepared by centrifuging the isolated paw tissue samples were prepared by centrifuging the isolated tissue homogenates (0.5 g) in 500 μL of cold PBS at 10000 rpm for 5 min at 4 °C. Similarly, the NO and H_2S levels of the foot tissue fluids were determined using Griess assay and WSP-5 probe.

2.19. Statistical analysis

All data are presented as means ± SD. The data were analyzed using *t*-test and one-way analysis of variance (ANOVA). $*P < 0.05$, $**P < 0.01$, $***P < 0.001$, $****P < 0.0001$ was considered significant, n.s. represents no significant difference. All statistical analyses were performed with GraphPad Prism software.

3. Results and discussion

3.1. Features of the pathology of rheumatoid arthritis

CIA is a widely used model of inflammatory arthritis for assessing the pathology and mechanisms of RA [30]. In addition, inflammation could activate macrophages, chondrocytes, and osteoclasts, exacerbating bone erosion in RA [31]. To investigate the inflammation and bone erosion in CIA rats, histological assays and micro-computed tomography (micro-CT) were used. We evaluated the inflammation of joints using immunofluorescence and immunohistochemistry (IHC). In contrast to the normal group, synovial hyperplasia and macrophage infiltration

were observed in the joint space of RA (Fig. 1a and b). In addition, the immunofluorescence results showed the increased infiltration of CD86 (M1 marker) macrophages. The IHC staining images further showed a high expression level of iNOS in the inflammatory synovium, which implies high NO level. Previous studies demonstrated that inflammation and macrophages could increase osteoclasts and bone erosion [5]. We examined the active osteoclasts using tartrate-resistant acid phosphatase (TRAP) staining. As shown in Fig. 1b, there are increased numbers of osteoclasts (black points), definitely narrowed joint space, and rough bone surfaces compared to that of normal rats. Additionally, the CIA rats were characterized by rough bone surfaces, severe bone erosion, markedly reduced bone mineral density (BMD), and increased bone surface area/bone volume (BS/BV) (Fig. 1c &d).

3.2. Synthesis and characterization of DNRS gel

HA is a biologically active molecule and the major component of articular cartilage, which could provide articular cartilage lubrication and protection [32,33]. Therefore, HA was adopted as the hydrogel backbone in this work. Firstly, HA-SH was synthesized by conjugating amino group by 3,3′-dithiobis (propanoic dihydrazide) according to previous work, subsequently reduced with tris (2-carboxyethyl) phosphine hydrochloride [34]. The HA-SH chemical structure was confirmed by ^{1}H NMR (Fig. S2). The trithiocarbonate RAFT agents could be used for conducting NO-responsive platforms as well as H_2S donors [27]. Then, we used an alkynyl-functionalized symmetrical trithiocarbonate chain transfer agent (CTA) to mediate the polymerization of poly (ethylene glycol) methyl ether acrylate and NO-responsive N-(2-aminophenyl) acrylamide hydrochloride (where m represents the feed molar ratio between poly(ethylene glycol) methyl ether acrylate and N-(2-aminophenyl) acrylamide hydrochloride (Figs. S3 and 4). The copolymer that could deplete NO and release H_2S was named as DNRS. The successful synthesis of the polymer was confirmed by gel permeation chromatography (GPC) (Fig. S5). The DNRS copolymer could self-assemble into spheres with an average particle size of about 60 nm, as confirmed by TEM and DLS (Fig. S6).

The DNRS gel can be rapidly gelated through a thiol-alkynyl "click" reaction between yne-DNRS copolymer and HA-SH (Fig. 2a), and its successful synthesis was demonstrated by ^{1}H NMR (Fig. S7). Peaks

identified in the XRD data indicate an amorphous structure in the hydrogels (Fig. S8), aligning with the typical structure of organic compounds. The optimized DNRS hydrogel was prepared with a polymer content (3 wt% in water) and a HA-SH: DNRS copolymer (weight ratio of 80:20) at room temperature. The storage modulus of prepared hydrogel was similar to the artificial intra-articular hydrogels for the treatment of arthritis [12]. The SEM images implied that the obtained DNRS hydrogels presented a porous network structure from freeze-dried approach (Fig. 2b). We next demonstrated the rheological properties of the gels at high strains by oscillatory rheological measurement (step-strain from ε = 0.5%–200%, ω = 10 rad s^{-1}) (Fig. 2c). Moreover, frequency-dependent rheological was determined to study the mechanical properties of DNRS gel (ε = 0.5%) (Fig. 2d). We found that the characterization of hydrogel did not change significantly with pH/temperature variation but gradually increased with elevated concentration, as well as the incorporation of MTX (Fig. S9). The recovery of the mechanical properties of the hydrogel might be mainly driven by the hydrophobic interactions of DNRS (Fig. 2e). A non-functional control (Ctrl) gel was prepared with alkyne-PEG-alkyne. Contrary to the Ctrl gel, the DNRS gel reduced the NO content from 36.9 μm to 16.5 μm and significantly increased the fluorescence intensity of H_2S (detected with WSP-5 probe) after the addition of cysteine (Fig. 2f–g & Fig. S10), DNRS gel swelled up after incubation with NO and cysteine (Fig. 2h). Furthermore, DNRS gel showed higher swelling and degradation rates in both NO and cysteine solutions, and lower in PBS (Fig. 2i–j). The explanation for these interesting phenomena is that DNRS gel could not only react with NO because of the contained NO-responsive o-PDA group, but also release H_2S as well as break the backbone due to the trithiocarbonate group (Fig. 2k) [27]. Interestingly, the degradation of the DNRS gel occurred with continuous cysteine exposure and subsequent to ~10 μm particles (Fig. 2l).

Based on the NO- and cysteine-responsive properties of DNRS gel, firstly, the gel could swell and become more porous with the presence of NO, which implies the gel could be used for the fabrication of NO-controlled drug delivery systems. Secondly, the backbone of cross-linker could be broken by cysteine, which intensifies the decomposition of the hydrogel and thus facilitates the release of drugs. Moreover, as the gel contained hydrophilic HA and multifunctional hydrophobic cross-linker, we anticipate that this gel also displays efficient drug-
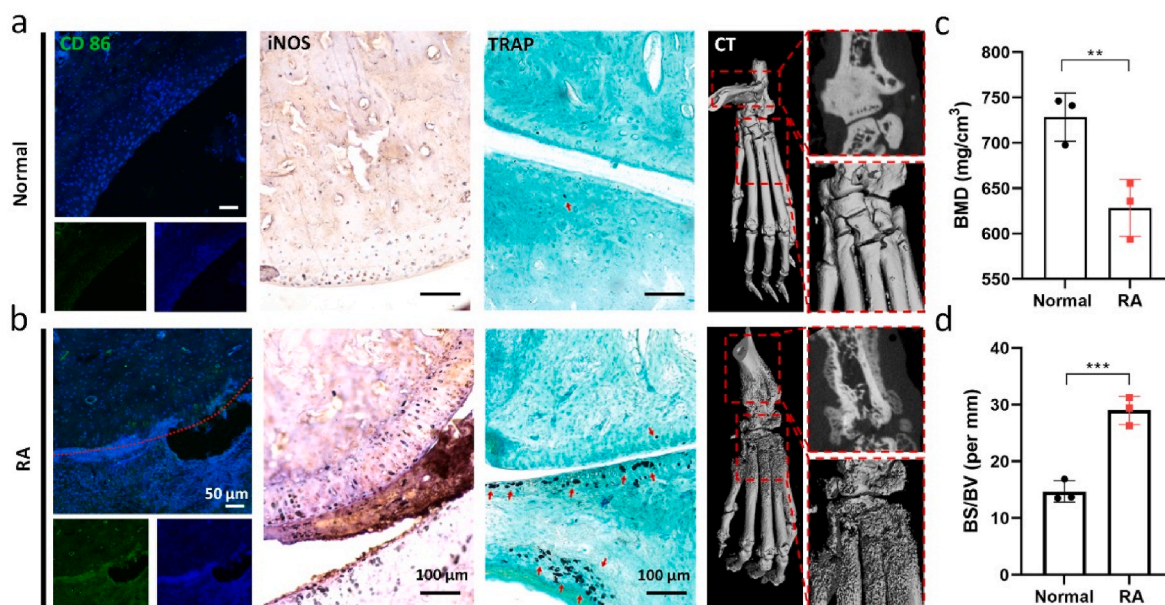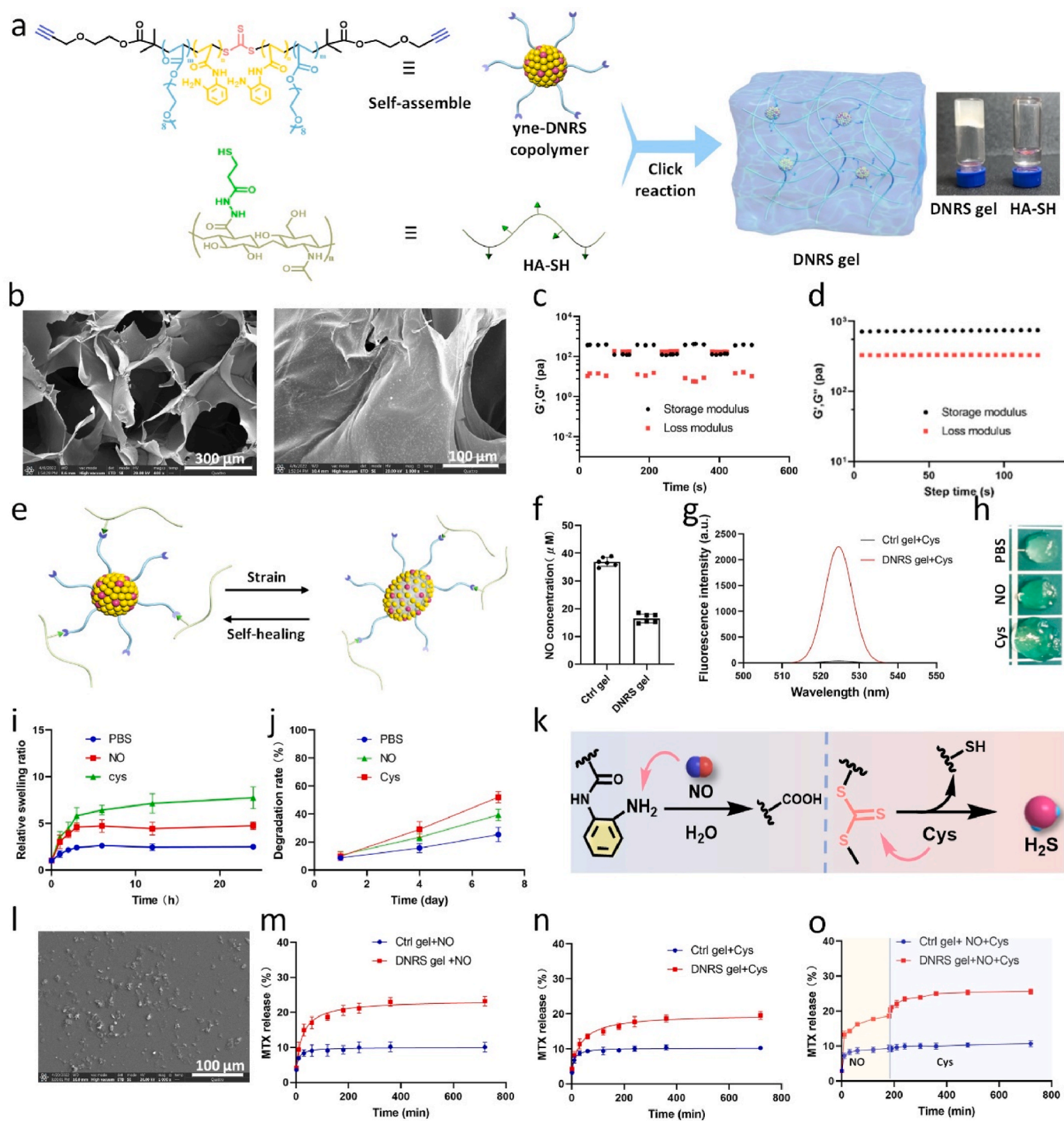

Fig. 1. Pathological features of rats in CIA and normal groups. a, b) immunofluorescence analyses of CD86 macrophages (green), immunohistochemical analyses, iNOS expression, and TRAP staining of osteoclast number in joints, micro-CT images of ankles respectively. c, d) Quantitative micro-CT analysis of BMD and BS/BV (n = 3). **$P < 0.01$, ***$P < 0.001$.

Fig. 2. Characterization of DNRS gel. a) The polymerization mechanism and photograph of DNRS gel. b) SEM images of DNRS gel. c) Step-strain oscillatory rheology of the self-healing DNRS gel (Step-strain from $\varepsilon = 0.5\%$–200%, angular frequency = 10 rad s^{-1}, 25 °C). d) Time-sweep rheological properties for DNRS gel ($\varepsilon = 0.5\%$, angular frequency = 10 rad s^{-1}, 25 °C). e) Schematic illustration of the self-healing gel, hydrophobic cross-linkers in gels can be reconnected under physical strain. f) The NO scavenging and g) H$_2$S releasing of DNRS gel. h) The DNRS gel images after 4 h incubation in PBS, NO solution (40 μM), and cysteine solution (100 μM). i) Relative swelling and j) degradation rates of DNRS hydrogels in PBS, NO solution (40 μM), and cysteine solution (100 μM) at different times, respectively. k) The working principle of DNRS gel. It depletes NO *via* the transformation of *o*-phenylenediamine into carboxyl and releases H$_2$S by the cysteine-triggered H$_2$S donor. l) The SEM images of the degraded DNRS gel. MTX red-loaded DNRS gel and Ctrl gel release profile after incubation with m) NO solution, n) cysteine, and o) NO and cysteine.

loading properties. The DNRS hydrogel loaded hydrophobic MTX with a loading efficiency of ~41% and loading content of ~6.5%, which were measured by NanoDrop 2000 at a wavelength of 208 nm. As shown in Fig. 2m–o, the DNRS gel could release MTX with NO or cysteine

exposure, and continuously release drug with the extra addition of cysteine, demonstrating its NO and cysteine responsive properties. The FTIR spectrum of hyaluronic acid component in DNRS gel exhibited peaks at 1640 cm^{-1} and 1020 cm^{-1}, however, peaks of 1200 cm^{-1} and

580 cm^{-1} for MTX were absent in the FTIR spectrum of MTX/DNRS gel (Fig. S11). This result indicated that no new chemical bonds were formed between MTX and the DNRS gel. Therefore, DNRS gel could release drugs under NO and cysteine with swell and erosion-based diffusion.

3.3. Anti-inflammation and macrophage polarization modulation by DNRS gel in vitro

The nano-size of DNRS copolymer may have a potential toxicity risk in cells, as shown in Fig. S12, the addition of 0.4 mg/mL of DNRS copolymer revealed a significant decrease in the viability of RAW264.7 cells, which was because DNRS could easily be engulfed by cells. The biocompatibility of DNRS can be greatly improved by cross-linking DNRS with HA. It was demonstrated that the two predominant cell types in joints are osteoblasts and macrophages [5]. Therefore, we first evaluated the cytotoxicity of DNRS gel and Ctrl gel for macrophage cells (Fig. 3a), the negligible cytotoxicity of DNRS and Ctrl gels was found even at high concentrations (2 mg/mL). Live/dead staining and CCK-8 also revealed the cell viability in macrophages and osteoblasts (Fig. 3b and Fig. S13). Both DNRS and Ctrl gels showed good cell growth conditions. This is mainly attributed to the great biocompatibility of HA.

Although NO and H_2S exhibit concentration-dependent biological effects. For RA, the level of NO and H_2S was dysregulated and excessive NO and deficient H_2S induced inflammation in the joint site [13,27]. Thus, the gel is expected to restore the inflammatory microenvironment *via* depleting NO and releasing H_2S. To assess the NO-scavenging and H_2S-releasing of DNRS gel with LPS-activated RAW264.7 cells *in vitro*, WSP-5 (H_2S probe, red) and DAF-2 (NO probe, green) were used. As shown in Fig. 3c, upon treatment with LPS, a certain increase in NO level but a decrease in H_2S level were observed, the levels of H_2S and NO returned to near physiological conditions. Then, the fluorescence intensity was counted with image J as shown in Fig. 3d &e. The H_2S concentration after LPS treatment was only 29.5% of the PBS group and then recovered to 130% after DNRS gel treatment. The NO level increased 13.5-fold after LPS treatment and then decreased 2.64-fold after DNRS gel treatment.

High TNF-α and IL-6 levels are closely relevant to RA progression. As in physiological disorders, excessive NO could induce the secretion of pro-inflammatory factors in macrophages. Thus, pro-inflammatory (TNF-α and IL-6) and anti-inflammatory cytokines (IL-10) were investigated by ELISA assays after different treatments (Fig. 3f–h). In good agreement with the immunofluorescence results, the results showed that the DNRS gel exhibited the best performance in reducing the TNF-α and IL-6 levels, whereas, an opposite trend was observed for anti-inflammatory (IL-10) cytokine, suggesting the combinatorial therapeutic effects of NO-depleting and H_2S-releasing.

A previous study has revealed that the pro-inflammatory M1 phenotype macrophage may exacerbate inflammation and promote osteoclast formation [35]. Notably, in the chronic inflammatory microenvironment of RA, dysfunctional macrophages do not polarize smoothly from M1 to M2, which prompted us to investigate whether the gel was capable of regulating macrophage polarization. As shown in Fig. 3j and Fig. S14, an increased M2 marker CD206 emission was found in LPS-activated macrophages, whereas the M1 marker CD86 emission was essentially unchanged. Meanwhile, the DNRS gel treatment gave rise to a marked decrease of CD86 expression and an increase of CD206 level in comparison with the LPS group. Moreover, LPS-stimulated macrophages showed short and filiform pseudopodia morphology, the elongated morphology of macrophages treated with DNRS gel verified the M2 type. Subsequently, flow cytometry analysis was further performed to assess macrophage polarization (Fig. 3i), LPS treatment significantly elevated the proportion of CD86 (3.90% *vs.* 17.6%) and CD206 (2.11% *vs.* 7.66%). After DNRS gel treatment, the expression level of CD206 was further increased to 23.7% and the expression level of CD86 decreased to 4.70%. Whereas, no obvious change in the

expression level of CD206 or CD86 was found between the LPS and Ctrl gel. These results demonstrated that DNRS gel successfully promoted macrophage polarization from M1 phenotype to M2 phenotype.

To find out how DNRS gel affects the immune microenvironment, RNA sequencing analysis was performed on LPS-activated RAW264.7 cells incubated with PBS (LPS group) and DNRS gel (DNRS gel group). Compared to the LPS group, 1232 differentially expressed genes were found in DNRS gel group and shown in the cluster heatmap, including 1074 up-regulated genes and 158 down-regulated genes ($p < 0.001$) (Fig. S15). Furthermore, Gene Ontology (GO) and Kyoto Encyclopedia of Genes and Genomes (KEGG) enrichment analyses were performed. The deferentially expressed genes revealed that they are mainly related to inflammatory responses, antigen processing and presentation, and immune system processes (Fig. 3k). KEGG pathway enrichment analysis showed many pathways, including macrophage cell differentiation, NF-κB signaling, and sulfur metabolism, play an important role (Fig. 3l). Collectively, these results implied that DNRS gel regulated endogenous gas signaling molecules, which in turn regulate macrophage cell differentiation and NF-κB pathway, then shaping the immune microenvironment to improve the treatment. Overall, the DNRS gel reduced inflammation and activated immunomodulatory effects to suppress M1 polarization, while promoting M2 macrophage polarization (Fig. 3m).

3.4. Osteogenic potential of DNRS gel

Subsequently, we illuminated the logic of bone metabolism and the inflammatory microenvironment. *In vitro* results show that LPS induced endogenous gas dysregulation *in vivo*, leading to an overproduction of pro-inflammatory factors and generating a severe inflammatory microenvironment. In turn, the pro-inflammatory factors could stimulate gas secretion by macrophages, forming a vicious circle that exacerbates the RA microenvironment. With the characterization of microenvironment-responsive releasing functionality of DNRS gel, not only excessive inflammatory factors could be depleted but also anti-inflammatory H_2S can be released, thereby promoting the polarization of M1 macrophages to M2 macrophages. DNRS gel could break the vicious circle of the RA microenvironment and restore the balance between osteoblasts and osteoclasts, paving the way for the healing of bone erosion.

Recent research has revealed that bone erosion is the consequence of an imbalance in the activity of osteoclasts and osteoblasts, and the anti-inflammatory M2 phenotype can induce an osteogenic microenvironment that improves osteogenesis [5,36]. Thus, we next sought to assess its osteogenic effect on osteoblasts under inflammatory microenvironment using the conditional medium of LPS-stimulated macrophages (Fig. 4a). The osteoblastic differentiation of osteoblasts with different samples was evaluated by detecting alkaline phosphatase (ALP) and alizarin red staining. As shown in Fig. 4b and d, the inflammatory environment mitigated the osteogenic activities of osteoblasts, while the DNRS gel displayed remarkable restoration of their abilities. No significant changes were found in ALP and alizarin red staining on day 1 (Fig. S16). Simultaneously, enhanced ALP activity and mineralized nodules were also found in the DNRS gel group, suggesting the DNRS gel is osteo-inductive and promotes osteoblasts' osteogenic activity by regulating the immunoregulatory effect *in vitro* (Fig. 4c &e). To further confirm the above results at the molecular level, the corresponding osteogenic genes including ALP, type I collagen (Col I), and osteocalcin (OCN)) were measured by enzyme-linked immunosorbent assay (ELISA) (Fig. 4f–h), respectively. As expected, the highest expression of osteogenic genes was found in DNRS gel group. Taken together, these results demonstrated that inflammation suppressed osteogenic activities and the dual-gas-mediated DNRS gel could promote the osteogenic expression of osteoblasts.

Increased osteoclast activity is the key factor that results in bone loss and joint destruction in osteoporosis and RA [37]. To investigate the potential of hydrogels to resist osteoclast differentiation, the morphology of macrophages after 3 days of culture in osteoclast
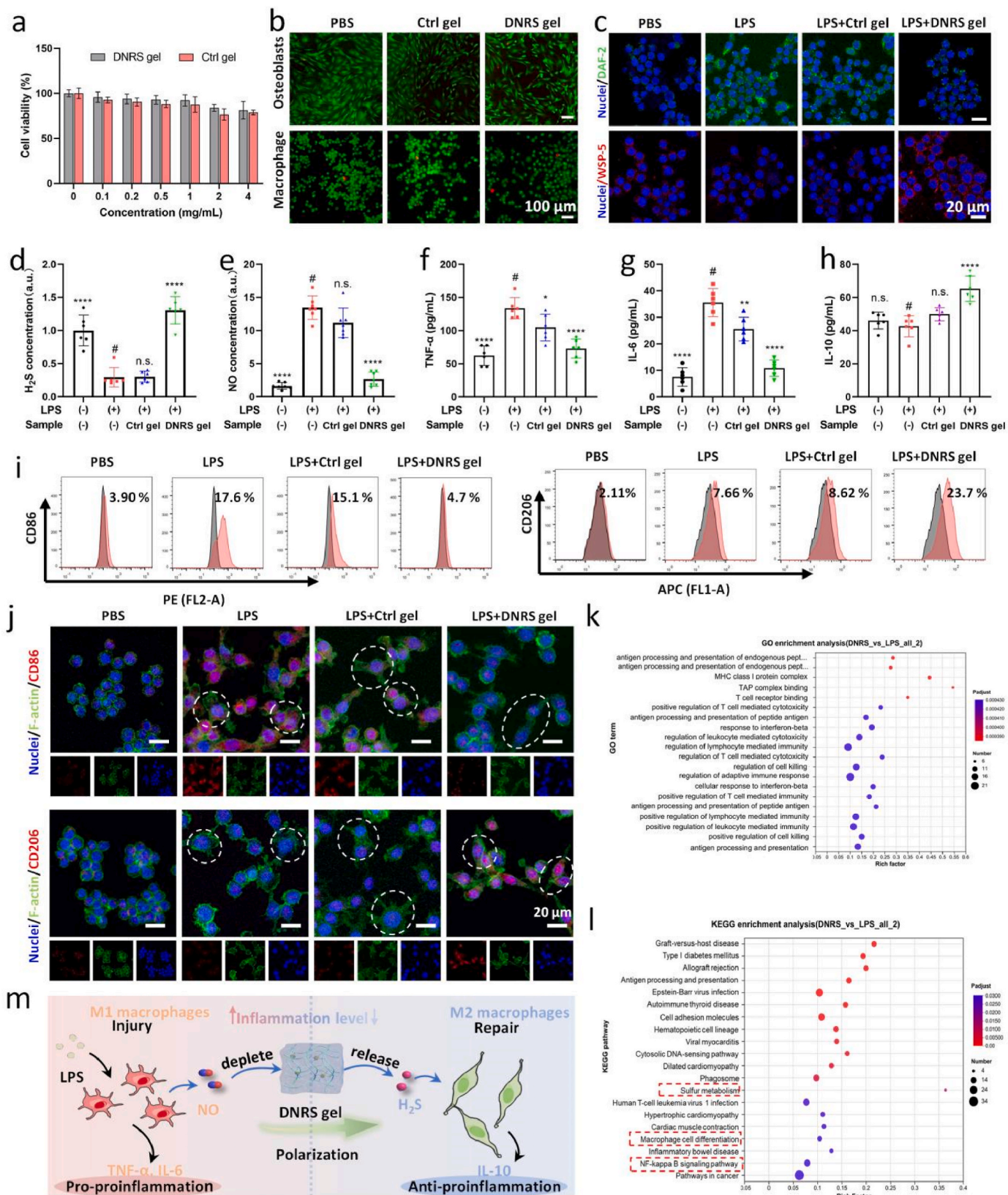
Fig. 3. *In vitro* anti-inflammation effects of DNRS gel. a) RAW264.7 viability was determined using CCK-8 assay for 24h treatment with DNRS gel and Ctrl gel at various concentrations (n = 4). b) Live/dead staining of macrophages and osteoblasts treated with Ctrl gel and DNRS gel. c) Intracellular NO level and H_2S level in LPS-activated macrophages treated with Ctrl gel and DNRS gel (n = 4). The corresponding fluorescence intensities of d) H_2S and e) NO in macrophages after different treatments. f-h) TNF-α, IL-6, and anti- IL-10 levels of different groups (n = 5). i) The CD86 and CD206 expression levels of macrophages after different treatment by the flow cytometry analysis. j) Representative fluorescent images of CD86 and CD206 in macrophages after different treatments. Scale bar: 20 μm. k) GO enrichment and l) KEGG enrichment analyses within LPS and DNRS gel groups. m) The potential mechanism of anti-inflammation macrophage and macrophage polarization by depleting NO and releasing H_2S. n.s. represents not significant, *$P < 0.05$, **$P < 0.01$, ****$P < 0.0001$, comparison between # and other groups.
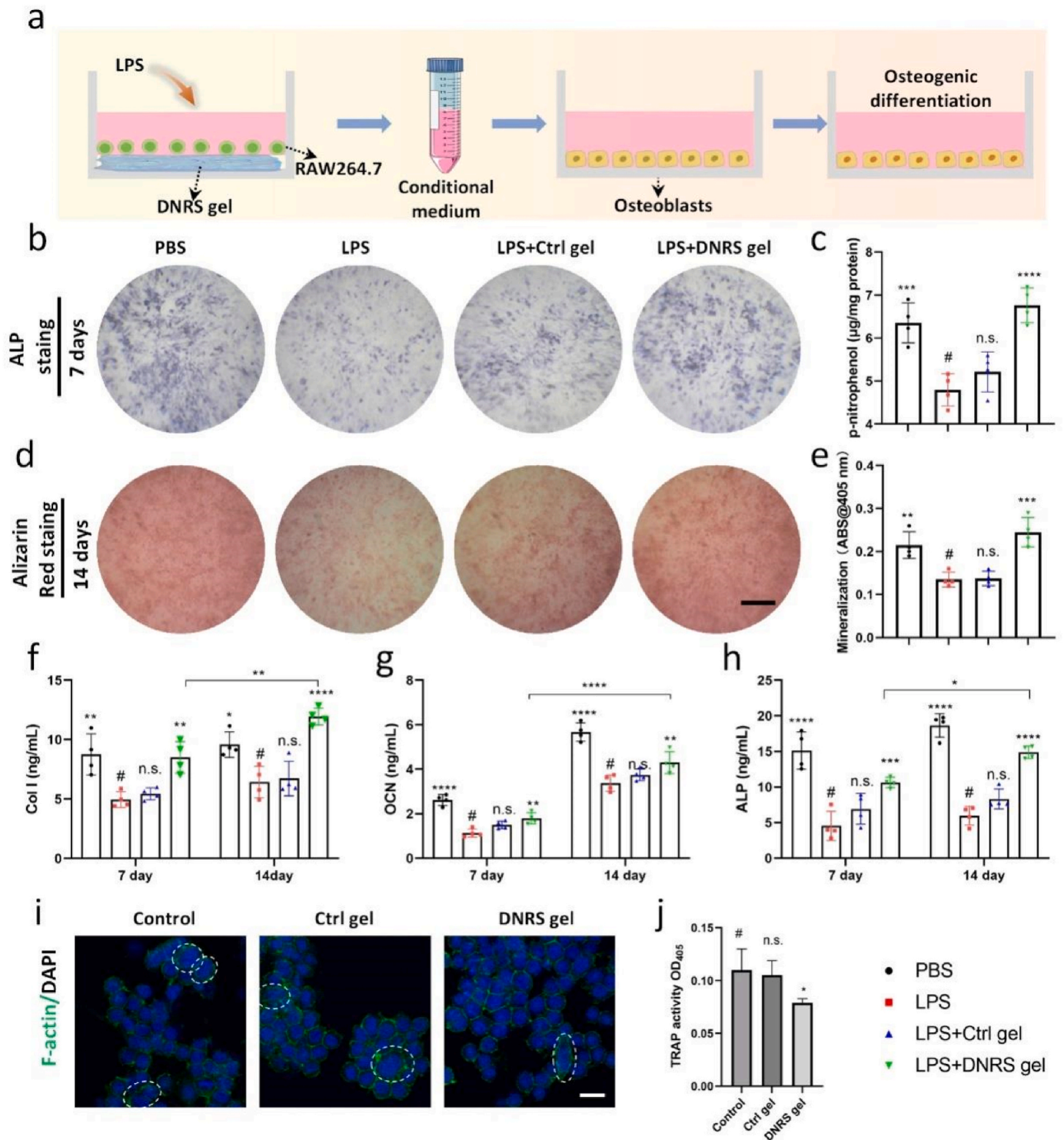
Fig. 4. DNRS gel improved the osteogenic potential under the inflammatory environment. a) The collection of conditional medium and osteoblasts processing method. Representative images of b) ALP staining and d) alizarin red staining of osteoblasts after treatment with different conditional media. Scale bar: 500 μm. Quantification analysis of c) ALP activity and d) mineralization. f-h) The levels of Col I, OCN, and ALP were measured by ELISA. i) CLSM images of multinucleated cells after different treatments for 3 days (green: F-actin; blue: nuclei). Scale bar: 20 μm. j) The production of TRAP of RAW264.7 cells after different treatments for 3 days. n = 4, n.s. represents not significant, *$P < 0.05$, **$P < 0.01$, ***$P < 0.001$, ****$P < 0.0001$.

induction medium was observed by CLSM. As shown in Fig. 4i, numerous multinuclear cells (osteoclasts, white circles) were easily found in the LPS and the Ctrl gel groups, while DNRS gel caused a reduction in osteoclasts. Furthermore. consistent with the DNRS gel significantly decreased osteoclast occurrence but not in the Ctrl gel group, as indicated by TRAP activity (Fig. 4j). The results demonstrated

the DNRS gel could inhibit the differentiation of osteoclasts. Therefore, the synergistic effect of the immunomodulation could promote osteogenesis and inhibit osteoclast proliferation by increasing the level of M2 polarization, reliving inflammatory microenvironment through the synergetic effects of NO-depletion and H_2S-generation on the DNRS gel.

3.5. Therapeutic efficacy of MTX/DNRS in vivo

Inspired by the drug-releasing capability, biocompatibility, and anti-inflammatory performance of the DNRS gel, we further studied the therapeutic effect of MTX-loaded DNRS gel on CIA rats. RA is a chronic inflammatory disease that joint swelling destruction with severe pain and impaired movement [6]. Before the investigation, the *in vivo* stability and biocompatibility of the DNRS gel were verified after its subcutaneous injection. As shown in Fig. S17a, the DNRS gel gelated immediately after injection, and there was little degradation and little change in hydrogel volume after 7 days. Furthermore, the body weight change and H&E staining of tissue indicated that DNRS gels had negligible toxicity and did not cause inflammation (Figs. S17b and c). When contacting with blood, DNRS gel should not induce hemolysis. The hemolysis ratios of all of the samples were lower than 5% (Fig. S18). A CIA rat model was constructed to evaluate the anti-inflammatory performance and bone protection of the injectable MTX/DNRS gel, the whole experimental procedure was shown in Fig. 5a. Arthritis was well developed within one week after boost immunization, CIA rats were randomized to five groups and their clinical scores, body weight, and thermographic images were monitored after treatment. The therapeutic effects were evaluated by clinical scores (Fig. 5b) [38]. Clearly, the MTX/DNRS gel group not only relieved RA symptoms, but also delayed the disease progression, and revealed remarkable improvements compared to the CIA model, MTX, and DNRS gel groups. The DNRS gel group exhibited certain therapeutic effects, not as effective as the MTX/DNRS gel group. The rats treated with MTX/DNRS gel showed high body weight (Fig. 5c). There was no significant relief in MTX group possibly owing to their rapid clearance *in vivo*.

Moreover, severe inflammation would cause the elevation of paw temperature. The temperature trends of the paws were measured by an infrared thermal imaging system after treatment with different groups. Thermographic images and temperature trends were shown in Fig. 5d and e. The results revealed that the paw temperature of the model group increased rapidly from 24.9 °C to 34.1 °C, and Ctrl gel group exhibited similar trend. Meanwhile, the paw temperature of the DNRS gel group increased slowly from 24.6 °C to 27.2 °C, and the MTX/DNRS gel group even showed decreased temperature from 24.0 °C to 23.6 °C, suggesting the temperature returned to normal. Interestingly, the higher the paw temperature, the more noticeable swelling, as inflammation is known to lead to an increase in temperature in the inflamed joints [39]. The swelling volume of the hind paws showed the same trend as the temperature changes (Fig. S19a). There was better recovery of motor ability in MTX/DNRS gel group (Fig. S19b), which is consistent with the clinical score and temperature trends.

Furthermore, H&E staining of synovium shows severe hyperplasia and a high number of leukocyte infiltration in the model group (Fig. 5f). while treated with saline H&E staining of ankles joints showed serious destruction of bone surface in the model group, and the residual joint space was invisible (Fig. 5g). And in the MTX group, the hyperplasia synovium adheres to the bone surface. In contrast, the MTX/DNRS gel group showed negligible bone destruction. To more deeply investigate the bone protection effect of the gel, Masson staining of ankles demonstrated that there was more collagen deposition when treated with MTX/DNRS gel than other groups. Additionally, we also evaluated the treatment of MTX/Ctrl gel, as shown in Fig. S20, the therapeutic efficacy of MTX/Ctrl gel is suboptimal. This may be due to the inability of the hydrophilic Ctrl gel to load a sufficient amount of hydrophobic MTX. Overall, the MTX/DNRS gel was demonstrated to effectively eliminate the symptoms of RA in CIA rats.

3.6. Anti-inflammation and macrophage polarization of MTX/DNRS gel in vivo

Macrophages in RA joints are mostly M1 phenotype, promoting RA progression via releasing various pro-inflammatory cytokines. Next,

whether DNRS gel could effectively drive the polarization of M1 macrophages was further investigated. The immunofluorescence of iNOS (pro-inflammation, M1) and CD206 (anti-inflammation, M2) in the inflammatory joints was measured. As shown in Fig. 6a and Fig. S21, the MTX/DNRS gel group had a strong fluorescence signal of CD206 macrophages and a faint fluorescence signal of iNOS macrophages, indicating a distinct transition of macrophage phenotype from a pro-inflammatory M1 phenotype to an anti-inflammatory M2 phenotype after MTX/DNRS gel treatment. Meanwhile, both the DNRS gel and MTX/DNRS gel groups decreased the ratios of iNOS$^+$ M1 macrophages as compared to the Ctrl gel and model groups, but the MTX/DNRS gel group displayed higher ratio of CD206$^+$ M2 macrophages. Hence, the DNRS gel potently relieved the unfavorable pro-inflammatory microenvironment by polarizing M1 phenotype macrophages to M2 phenotype *in vivo*.

To further confirm the anti-inflammatory property of DNRS gel *in vivo*, the expression levels of pro-inflammatory cytokines and anti-inflammatory cytokines were measured via ELISA and immunofluorescence staining in RA joints, which are tightly correlated with RA progression [7,8]. As displayed in Fig. 6b–g, The DNRS gel and the MTX/DNRS gel significantly decreased the levels of TNF-α and IL-6, in comparison with the MTX group and model group in both serum and foot tissue fluids, suggesting a low immune response to relieve inflammation. Conversely, the level of IL-10 of the MTX/DNRS gel group was higher than that of the free MTX and gel groups. Likewise, the expression of TNF-α and IL-10 of the inflammatory joint was evaluated by immunofluorescence staining (Fig. S22) and similar results were obtained. In addition, endogenous gas (NO and H$_2$S) levels have returned to normal levels in the joint synovial fluid (Fig. 6h–i). The DNRS gel significantly improves the inflammatory microenvironment of RA, breaking the vicious circle of the RA microenvironment, and paving the way for the healing of bone erosion.

3.7. Bone protection of MTX/DNRS gel in vivo

The inflammatory microenvironment often causes imbalance in bone metabolism, which in turn leads to increased bone erosion. Successful bone protection is inseparable from the balance between osteoclasts and osteoblasts [40]. We next evaluated the levels of osteoclasts and osteoblasts in inflamed joints via immunohistochemical staining of osteogenesis-related markers (ALP, Col I, and OCN) and TRAP staining of osteoclasts. As shown in Fig. 7a–e, the level of ALP after the MTX/DNRS gel treatment exhibited the highest than that of the free MTX and DNRS gel group, near normal levels. While the DNRS gel alone was not sufficient, the combination with MTX dramatically improved the protection of osteogenesis. The level of OCN and Col I also showed similar results, and more importantly, the expected increases in osteoclast number in RA were significantly suppressed by the MTX/DNRS gel treatment. No differences were found in the CIA rats treated with MTX or free DNRS gel.

As the CIA rats were characterized by rough bone surfaces, severe bone erosion, markedly reduced bone mineral density (BMD) and increased bone surface density (BS/BV), we assessed the bone protection effects of the DNRS gel. The joint morphologies were investigated by micro-CT (Fig. 7f–h) on day 28. Smooth bone surfaces, increased BMD, and decreased BS/BV were observed in the DNRS gel and the MTX/DNRS gel groups, validating the efficient bone protection of the hydrogel. DNRS gel showed slight efficacy in reducing bone erosion. The MTX group revealed limited effectiveness in reducing bone erosion (Fig. 7h). Additionally, MTX/DNRS gel treatment could most effectively increase BV/TV while decreasing (Tb. Sp) (Fig. S23). These results demonstrated the efficient control of osteoporosis in RA, which was mainly caused by osteoclast suppression induced by MTX/DNRS gel, effectively restoring the microenvironment of RA and the bone metabolism. Taken together, the designed DNRS gel displayed a potential therapeutic approach for CIA-induced bone erosion and inflammation-
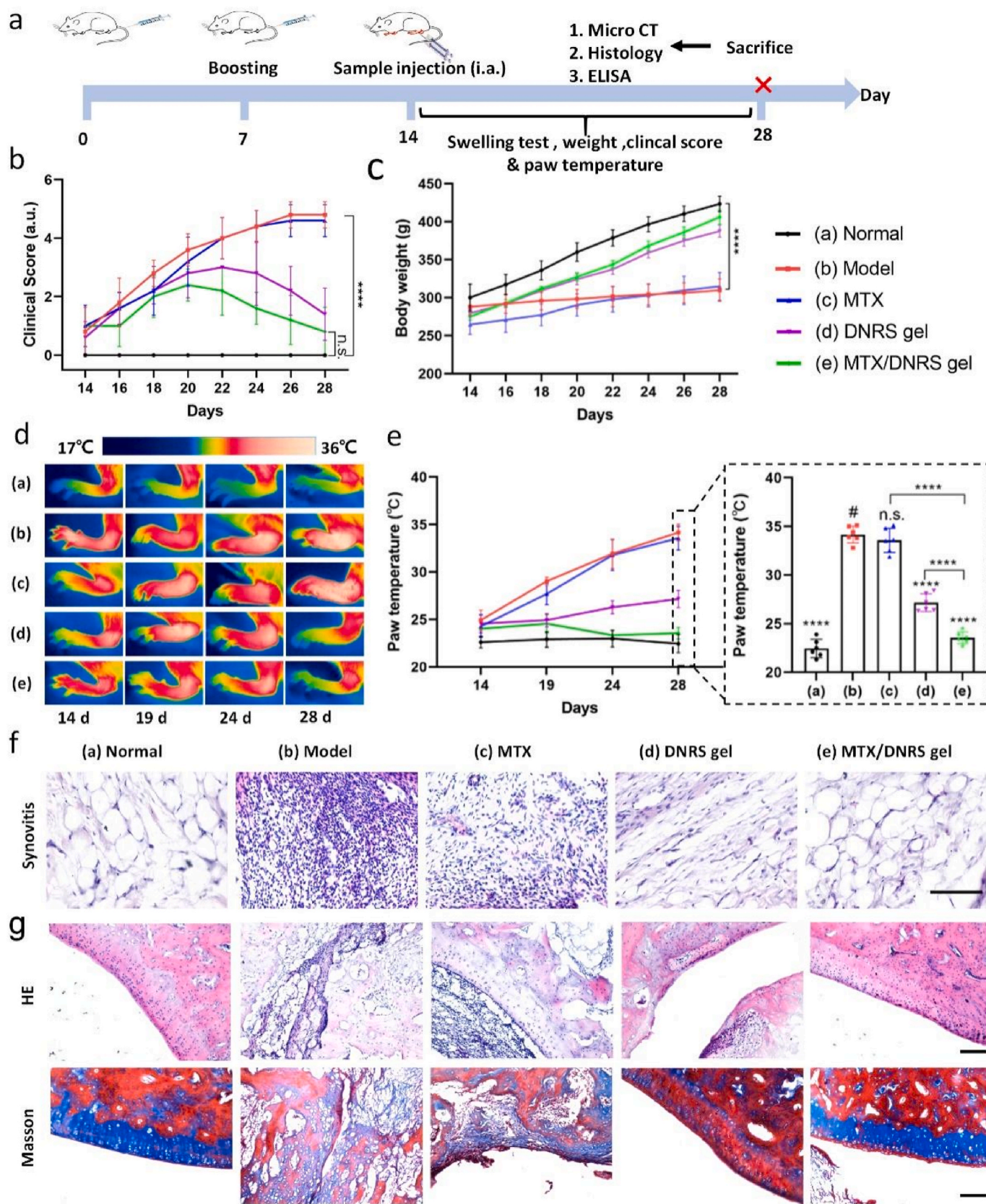
Fig. 5. *In vivo* therapeutic effects of DNRS gel. a) Experimental timeline of gel treatment. b) Clinical score and c) body weight of CIA rats for different groups. d) Thermographic images and e) temperature of inflammatory joints after various treatments on different days. f) H&E staining of synovium. g) H&E and Masson staining of ankle joints. Scale bars: 100 μm. n = 6, n.s. represents not significant, *P < 0.05, **P < 0.01, ***P < 0.001, ****P < 0.0001.
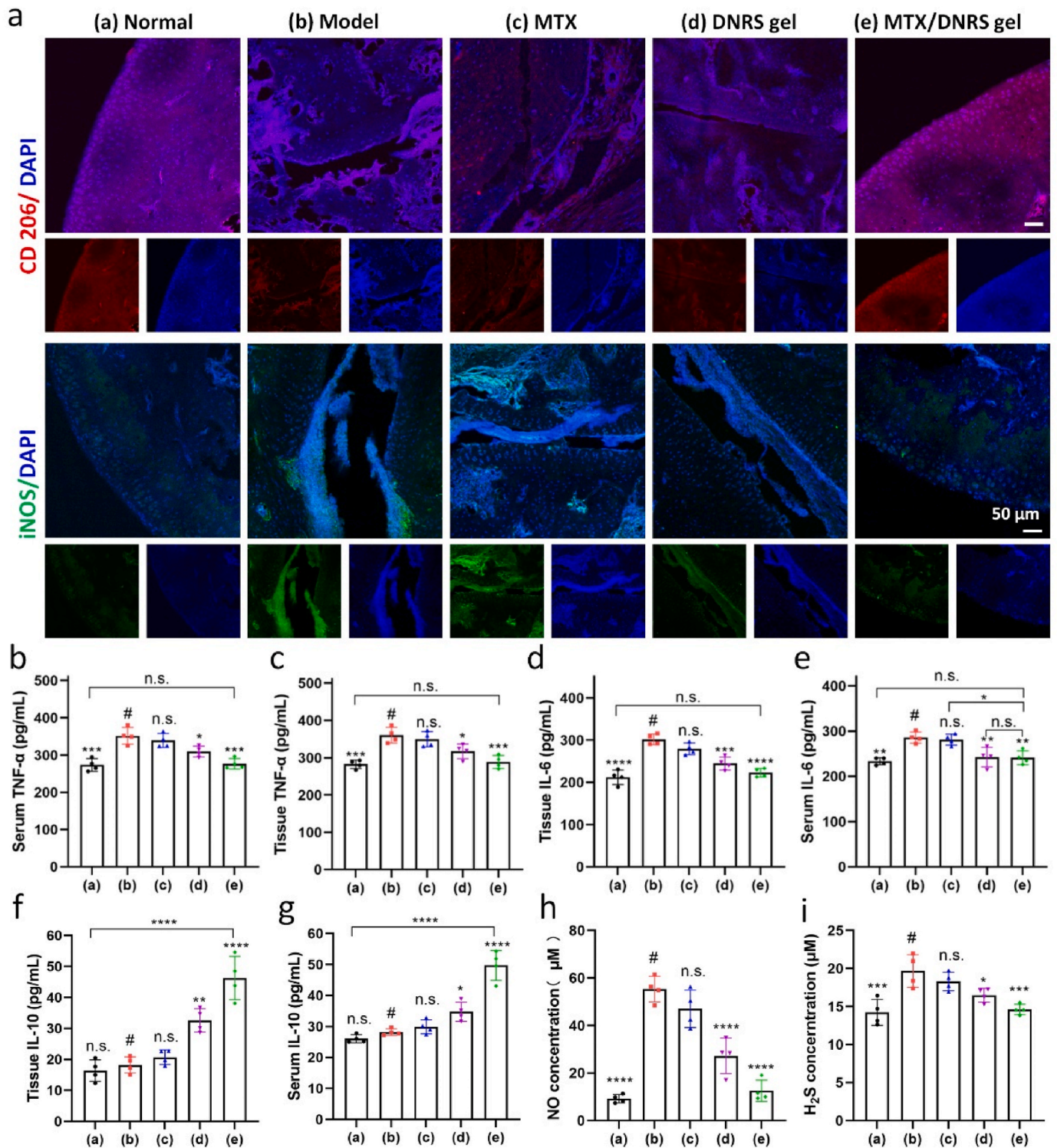
Fig. 6. *In vivo* anti-inflammatory effects of MTX/DNRS gel. a) The immunofluorescence staining of CD206 and iNOS in the joints of different groups. Scale bar: 50 μm. b-g) The secretion of TNF-α, IL-6, and IL-10 in the serum and tissues of different groups. h-i) NO and H_2S concentration in the joint synovial fluid at day 28. n = 4, n.s. represents not significant, *$P < 0.05$, **$P < 0.01$, ***$P < 0.001$, ****$P < 0.0001$ comparison between # and other groups.

related osteoporosis.

4. Conclusions

In summary, we have successfully developed a self-healing injectable multifunctional hydrogel by metal-free click reaction for restoring RA microenvironment, which could scavenge pro-inflammatory NO and release anti-inflammatory H_2S while continuously releasing drugs. Our *in vitro* results demonstrated that this gel was efficient at inducing macrophages to undergo M2 polarization, restraining inflammation, promoting osteogenic activity in osteoblasts and suppressing osteoclastogenesis. In a CIA rat model, the multifunctional drug-loading system also exhibited an outstanding anti-inflammatory effect, successfully postponed the progression of CIA joints and mitigated joint damage.
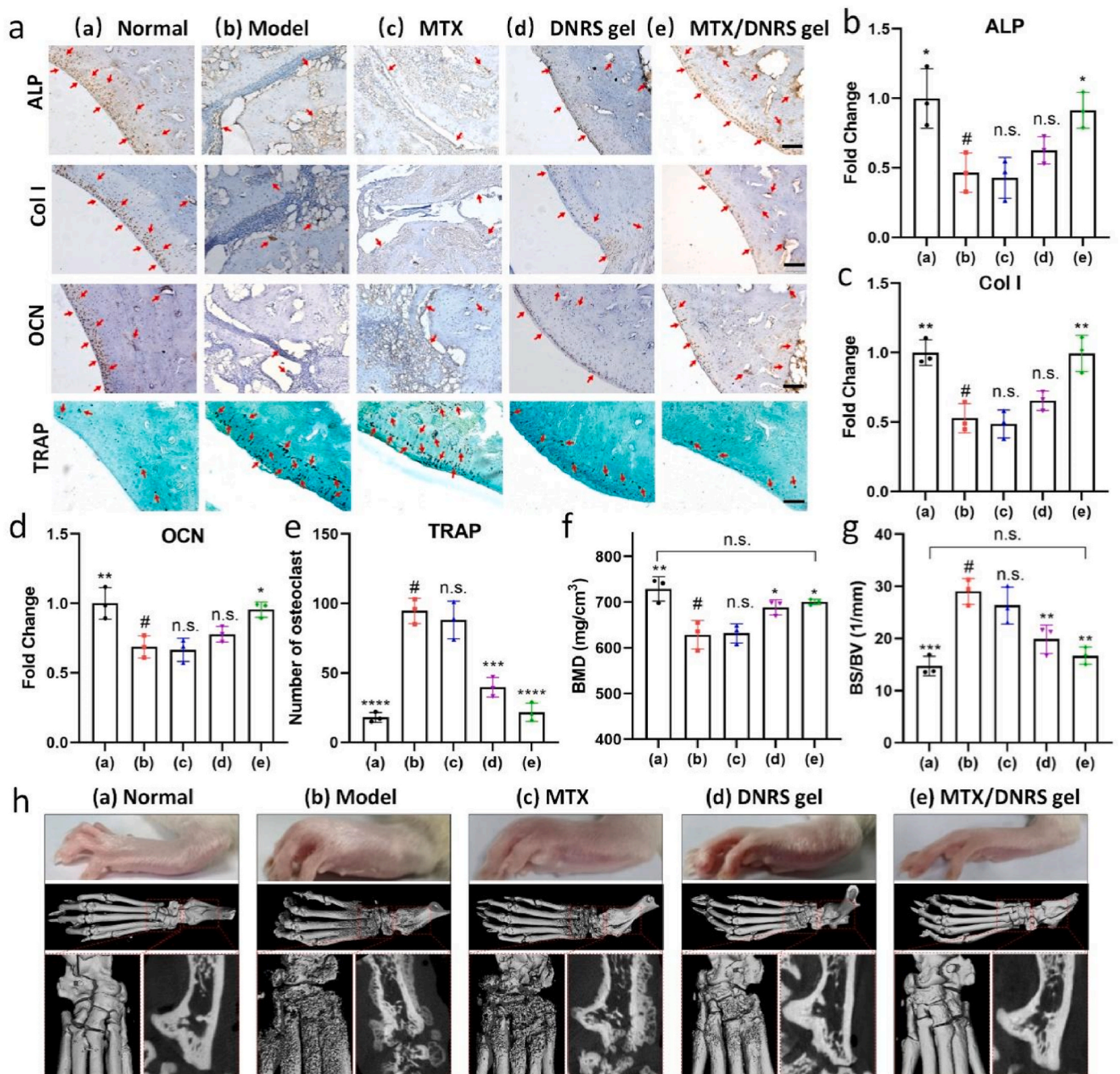
Fig. 7. Bone protection of MTX/DNRS gel in joints of CIA rats. a) ALP, Col I, and OCN expression levels and TRAP-stained osteoclasts in the joints in different groups. Scale bar: 100 μm. b-e) Statistics of ALP, Col I, OCN changes, and numbers of osteoclasts in the joints. f-g) BMD and BS/BV of RA rats received different treatments at day 28. h) Representative photographs and micro-CT images of RA rats received different treatments on day 28. n = 3, n.s. represents not significant, $*P < 0.05$, $**P < 0.01$, $***P < 0.001$, $****P < 0.0001$.

Collectively, our work not only provided a promising application potential for regulating endogenous gas levels to eliminate inflammation but also a better understanding of the impact of microenvironment on bone protection.

Ethics approval and consent to participate

All animal procedures were approved by Chongqing University's Laboratory Animal Welfare and Ethics Committee (CQU-IACUC-RE-202205-001).

CRediT authorship contribution statement

Wenbo Geng: Writing – original draft, Methodology, Formal analysis, Data curation. **Jie Zhao:** Validation, Software, Investigation, Formal analysis. **Bailong Tao:** Visualization, Validation, Formal analysis. **Yulu Yang:** Validation, Methodology, Formal analysis. **Qiaojian Duan:** Visualization, Methodology, Data curation. **Pengfei Gao:** Visualization, Software, Data curation. **Tingting He:** Methodology, Investigation, Data curation. **Shaopeng Liu:** Software, Methodology, Investigation. **Qian Feng:** Writing – original draft, Validation, Formal analysis. **Peng Zhao:** Validation, Methodology, Formal analysis. **Kaiyong Cai:** Writing – review & editing, Supervision, Resources,

Project administration, Conceptualization.

Declaration of competing interest

The authors declare that they have no known competing financial interests or personal relationships that could have appeared to influence the work reported in this paper.

Appendix A. Supplementary data

Supplementary data to this article can be found online at https://doi.org/10.1016/j.bioactmat.2024.03.002.

References

[1] Y. Zhu, T. Zhao, M. Liu, S. Wang, S. Liu, Y. Yang, Y. Yang, Y. Nan, Q. Huang, K. Ai, Rheumatoid arthritis microenvironment insights into treatment effect of nanomaterials, Nano Today 42 (2022) 101358.

[2] G.R. Burmester, J.E. Pope, Novel treatment strategies in rheumatoid arthritis, Lancet 389 (2017) 2338–2348.

[3] Y. Lu, Z. Li, L. Li, J. Chen, X. Xu, Z. Lin, T. Zhang, Y. Zhu, C. Ding, C. Mao, Highly effective rheumatoid arthritis therapy by peptide-promoted nanomodification of mesenchymal stem cells, Biomaterials 283 (2022) 121474.

[4] J. Meng, W. Zhang, C. Wang, W. Zhang, C. Zhou, G. Jiang, J. Hong, S. Yan, W. Yan, Catalpol suppresses osteoclastogenesis and attenuates osteoclast-derived bone resorption by modulating PTEN activity, Biochem. Pharmacol. 171 (2020) 113715.

[5] T. Gong, Z. Zhang, Targeted apoptosis of macrophages and osteoclasts in arthritic joints is effective against advanced inflammatory arthritis, Nat. Commun. 12 (2021) 2174.

[6] C.M. Weyand, J.J. Goronzy, Immunometabolism in early and late stages of rheumatoid arthritis, Nat. Rev. Rheumatol. 13 (2017) 291–301.

[7] D. Aletaha, J.S. Smolen, Diagnosis and management of rheumatoid arthritis: a review, JAMA 320 (2018) 1360–1372.

[8] K.M. Kingsmore, A.C. Grammer, P.E. Lipsky, Drug repurposing to improve treatment of rheumatic autoimmune inflammatory diseases, Nat. Rev. Rheumatol. 16 (2020) 32–52.

[9] M.H. Buch, S. Eyre, D. McGonagle, Persistent inflammatory and non-inflammatory mechanisms in refractory rheumatoid arthritis, Nat. Rev. Rheumatol. 17 (2021) 17–33.

[10] G. Nagy, N.M. Roodenrijs, P.M. Welsing, M. Kedves, A. Hamar, M.C. van der Goes, A. Kent, M. Bakkers, E. Blaas, L. Senolt, EULAR definition of difficult-to-treat rheumatoid arthritis, Ann. Rheum. Dis. 80 (2021) 31–35.

[11] W. Zhang, Q. Liu, M. Zhou, K. Wang, Y. Wang, J. Nie, S. Gui, D. Peng, Z. He, Emerging nanotherapeutics alleviating rheumatoid arthritis by readjusting the seeds and soils, J. Contr. Release 345 (2022) 851–879.

[12] T. Kim, J. Suh, W.J. Kim, Polymeric aggregate-embodied hybrid nitric-oxide-scavenging and sequential drug-releasing hydrogel for combinatorial treatment of rheumatoid arthritis, Adv. Mater. 33 (2021) 2008793.

[13] J. Yeo, Y.M. Lee, J. Lee, D. Park, K. Kim, J. Kim, J. Park, W.J. Kim, Nitric oxide-scavenging nanogel for treating rheumatoid arthritis, Nano Lett. 19 (2019) 6716–6724.

[14] J. Ma, C. Shi, Z. Liu, B. Han, L. Guo, L. Zhu, T. Ye, Hydrogen sulfide is a novel regulator implicated in glucocorticoids-inhibited bone formation, Aging (Albany NY) 11 (2019) 7537–7552.

[15] Y. Hao, H. Wang, L. Fang, J. Bian, Y. Gao, C. Li, H$_2$S donor and bone metabolism, Front. Pharmacol. 12 (2021) 661601.

[16] H. Kalyanaraman, N. Schall, R.B. Pilz, Nitric oxide and cyclic GMP functions in bone, Nitric Oxide 76 (2018) 62–70.

[17] F. Benedetti, S. Curreli, S. Krishnan, S. Davinelli, F. Cocchi, G. Scapagnini, R. C. Gallo, D. Zella, Anti-inflammatory effects of H$_2$S during acute bacterial infection: a review, J. Transl. Med. 15 (2017) 1–11.

[18] H. Liu, C.J. Rosen, Nitric oxide and bone: the phoenix rises again, J. Clin. Investig. 131 (2021) e147072.

[19] S. Tao, J. Cheng, G. Su, D. Li, Z. Shen, F. Tao, T. You, Breathing micelles for combinatorial treatment of rheumatoid arthritis, Angew. Chem. Int. Ed. 59 (2020) 21864–21869.

[20] Y. Li, H.Y. Yang, D.S. Lee, Advances in biodegradable and injectable hydrogels for biomedical applications, J. Contr. Release 330 (2021) 151–160.

[21] M. Wang, M. Chen, W. Niu, D.D. Winston, W. Cheng, B. Lei, Injectable biodegradation-visual self-healing citrate hydrogel with high tissue penetration for microenvironment-responsive degradation and local tumor therapy, Biomaterials 261 (2020) 120301.

[22] J. Park, S. Pramanick, D. Park, J. Yeo, J. Lee, H. Lee, W.J. Kim, Therapeutic-gas-responsive hydrogel, Adv. Mater. 29 (2017) 1702859.

[23] T. Kim, J. Suh, W.J. Kim, Polymeric aggregate-embodied hybrid nitric-oxide-scavenging and sequential drug-releasing hydrogel for combinatorial treatment of rheumatoid arthritis, Adv. Mater. 33 (2021) e2008793.

[24] R.S. Hsu, P.Y. Chen, J.H. Fang, Y.Y. Chen, C.W. Chang, Y.J. Lu, S.H. Hu, Adaptable microporous hydrogels of propagating NGF-gradient by injectable building blocks for accelerated axonal outgrowth, Adv. Sci. 6 (2019) 1900520.

[25] T. Kim, J. Suh, W.J. Kim, Polymeric aggregate-embodied hybrid nitric-oxide-scavenging and sequential drug-releasing hydrogel for combinatorial treatment of rheumatoid arthritis, Adv. Mater. 33 (2021) 2008793.

[26] K.P. McClelland, T.D. Clemons, S.I. Stupp, E.A. Weiss, Semiconductor quantum dots are efficient and recyclable photocatalysts for aqueous PET-RAFT polymerization, ACS Macro Lett. 9 (2019) 7–13.

[27] W. Geng, X. Liu, B. Tao, Y. He, K. Li, P. Gao, Q. Feng, P. Zhao, Z. Luo, K. Cai, Nitric oxide scavenging and hydrogen sulfide production synergistically treat rheumatoid arthritis, Adv. Healthcare Mater. (2022) 2202380.

[28] S.M. Lee, H.J. Kim, Y.J. Ha, Y.N. Park, S.K. Lee, Y.B. Park, K.H. Yoo, Targeted chemo-photothermal treatments of rheumatoid arthritis using gold half-shell multifunctional nanoparticles, ACS Nano 7 (2013) 50–57.

[29] W. Geng, M. Chen, B. Tao, R. Wang, D. Wang, K. Li, C. Lin, X. Liu, P. Gao, Z. Luo, K. Cai, Cell-free DNA depletion via cell-penetrating poly(disulfide)s for rheumatoid arthritis therapy, Appl. Mater. Today 26 (2022) 101351.

[30] P.V. Alabarse, P.S. Lora, J.M. Silva, R.C. Santo, E.C. Freitas, M.S. de Oliveira, A. S. Almeida, M. Immig, V.O. Teixeira, L.I. Filippin, Collagen-induced arthritis as an animal model of rheumatoid cachexia, J. Cachexia Sarcopenia Muscle 9 (2018) 603–612.

[31] I.B. McInnes, G. Schett, The pathogenesis of rheumatoid arthritis, N. Engl. J. Med. 365 (2011) 2205–2219.

[32] G. Chen, J. Guo, J. Nie, G. Ma, Preparation, characterization, and application of PEO/HA core shell nanofibers based on electric field induced phase separation during electrospinning, Polymer 83 (2016) 12–19.

[33] W. Gao, K. Chen, W. He, S. Zhao, D. Cui, C. Tao, Y. Xu, X. Xiao, Q. Feng, H. Xia, Synergistic chondrogenesis promotion and arthroscopic articular cartilage restoration via injectable dual-drug-loaded sulfated hyaluronic acid hydrogel for stem cell therapy, Compos. B Eng. (2023) 110857.

[34] M.M. Pérez-Madrigal, J.E. Shaw, M.C. Arno, J.A. Hoyland, S.M. Richardson, A. P. Dove, Robust alginate/hyaluronic acid thiol–yne click-hydrogel scaffolds with superior mechanical performance and stability for load-bearing soft tissue engineering, Biomater. Sci. 8 (2020) 405–412.

[35] J. Li, J. Wen, B. Li, W. Li, W. Qiao, J. Shen, W. Jin, X. Jiang, K.W. Yeung, P.K. Chu, Valence state manipulation of cerium oxide nanoparticles on a titanium surface for modulating cell fate and bone formation, Adv. Sci. 5 (2018) 1700678.

[36] J. Wu, P. Shen, X. Qin, Y. Yang, C. Lin, X. Li, W. Geng, P. Gao, L. Chen, L. Miao, Self-supply of H$_2$O$_2$ and O$_2$ by a composite nanogenerator for chemodynamic therapy/hypoxia improvement and rapid therapy of biofilm-infected wounds, Chem. Eng. J. 459 (2023) 141507.

[37] L.J. O'Neil, C.B. Oliveira, X. Wang, M. Navarrete, A. Barrera-Vargas, J. Merayo-Chalico, R. Aljahdali, E. Aguirre-Aguilar, P. Carlucci, M.J. Kaplan, Neutrophil extracellular trap-associated carbamylation and histones trigger osteoclast formation in rheumatoid arthritis, Ann. Rheum. Dis. 82 (2023) 630–638.

[38] S. Seeuws, P. Jacques, J. Van Praet, M. Drennan, J. Coudenys, T. Decruy, E. Deschepper, L. Lepescheux, P. Pujuguet, L. Oste, N. Vandeghinste, R. Brys, G. Verbruggen, D. Elewaut, A multiparameter approach to monitor disease activity in collagen-induced arthritis, Arthritis Res. Ther. 12 (2010) 1–10.

[39] P. Barragán-Iglesias, T.-F. Lou, V.D. Bhat, S. Megat, M.D. Burton, T.J. Price, Z. T. Campbell, Inhibition of Poly (A)-binding protein with a synthetic RNA mimic reduces pain sensitization in mice, Nat. Commun. 9 (2018) 10.

[40] B. Tao, C. Lin, Y. He, Z. Yuan, M. Chen, K. Xu, K. Li, A. Guo, K. Cai, L. Chen, Osteoimmunomodulation mediating improved osteointegration by OGP-loaded cobalt-metal organic framework on titanium implants with antibacterial property, Chem. Eng. J. 423 (2021) 130176.